Kaposi's sarcoma-associated herpesvirus fine-tunes the temporal expression of late genes by manipulating a host RNA quality control pathway

Julio C. Ruiz[1], Anne Devlin[1], Jiwoong Kim[2], Nicholas K. Conrad[1]*

[1]Department of Microbiology, [2]Department of Population and Data Sciences, University of Texas Southwestern Medical Center, Dallas, Texas, USA

Running title: PPD dampens KSHV late gene expression

*Corresponding author: Nicholas.Conrad@UTSouthwestern.edu

Abstract

Kaposi's sarcoma-associated herpesvirus (KSHV) is a human oncogenic nuclear DNA virus that expresses its genes using the host cell transcription and RNA processing machinery. As a result, KSHV transcripts are subject to degradation by at least two host-mediated nuclear RNA decay pathways, PABPN1 and PAPα/γ-mediated RNA decay (PPD) and an ARS2-dependent decay pathway. Here, we present global analyses of viral transcript levels to further understand the roles of these decay pathways in KSHV gene expression. Consistent with our recent report that the KSHV ORF57 protein increases viral transcript stability by impeding ARS2-dependent decay, ARS2 knockdown has little effect on viral gene expression 24 hours after lytic reactivation of wild-type virus. In contrast, inactivation of PPD results in premature accumulation of late transcripts. The up-regulation of late transcripts does not require the primary late gene-specific viral transactivation factor, suggesting that cryptic transcription produces the transcripts that then succumb to PPD. Remarkably, PPD inactivation has no effect on late transcripts at their proper time of expression. We show that this time-dependent PPD evasion by late transcripts requires the host factor NRDE2, which has previously been reported to protect cellular RNAs by sequestering decay factors. From these studies, we conclude that KSHV uses PPD to fine-tune the temporal expression of its genes by preventing their premature accumulation.

Importance

Kaposi's sarcoma-associated herpesvirus (KSHV) is an oncogenic gammaherpesvirus that causes Kaposi's sarcoma and other lymphoproliferative disorders. Nuclear expression of KSHV genes results in exposure to at least two host-mediated nuclear RNA decay pathways, PABPN1 and PAPα/γ-mediated RNA decay (PPD) and an ARS2-mediated decay pathway. Perhaps unsurprisingly, we previously found that KSHV uses specific mechanisms to protect its transcripts from ARS2-mediated decay. In contrast, here we show that PPD is required to dampen the expression of viral late transcripts that are prematurely transcribed, presumably due to cryptic transcription early in infection. At the proper time for their expression, KSHV late transcripts evade PPD through the activity of the host factor NRDE2. We conclude that KSHV fine-tunes the temporal expression of its genes by modulating PPD activity. Thus, the virus both protects from and exploits the host nuclear RNA decay machinery for proper expression of its genes.

Introduction

Kaposi's sarcoma-associated herpesvirus (KSHV; also known as human herpesvirus 8; HHV-8), is an enveloped, double-stranded DNA virus. It is the etiological agent of Kaposi's sarcoma and of the lymphoproliferative disorders primary effusion lymphoma (PEL) and multicentric Castleman's disease (MCD) (1-4). Like other herpesvirus, the KSHV life cycle consists of a latent phase and a lytic phase. During latency, the viral genome resides in the host nucleus as a non-integrated, circular episome, and no virions are produced. Upon reactivation, the virus undergoes a well-regulated cascade of gene expression initiated by the viral transactivator ORF50 (Rta) that ultimately results in the production of infectious virus (5-7). KSHV transcription and genome replication occur in the nucleus where the virus takes control of the host machinery needed for these processes. Consequently, similar to host RNAs, viral transcripts are subject to host-mediated RNA quality control (QC) pathways (8-12).

RNA QC pathways play an essential role during RNA biogenesis (8-12). In addition to eliminating misprocessed transcripts, RNA QC pathways prevent the accumulation of unstable, non-coding RNAs such as promoter-upstream transcripts (PROMPTs, also called uaRNAs) (13-15). PROMPTs are polyadenylated, non-coding RNAs with no or few introns that are transcribed from bidirectional promoters antisense to protein-coding genes (16-18). Accumulation of PROMPTs has deleterious effects for the cells as they compete with coding transcripts for the translational machinery (15). In eukaryotes, at least two nuclear RNA decay pathways prevent the accumulation of PROMPTs (13-15,

19, 20). Primarily, they are degraded through the CBCN complex that is recruited to the RNA via its 5´ cap. CBCN consists of the cap-binding complex (CBC), the ARS2 protein, and the nuclear exosome targeting (NEXT) complex (13, 21). The NEXT complex subunit MTR4 recruits the RNA exosome to degrade the transcript (13, 22).

PROMPTs and other long polyadenylated nuclear RNAs are also degraded by the PABPN1 and PAPα/γ-mediated RNA decay (PPD) pathway in which decay factors are recruited through 3´ poly(A) tail (14, 15, 19, 20, 23, 24). In this pathway, the nuclear poly (A)-binding protein (PABPN1) promotes poly(A) tail extension of target transcripts by stimulating the function of the poly (A) polymerases (PAPα or PAPγ; abbreviated PAPα/γ). The targeted RNAs are subsequently degraded by the nuclear RNA exosome. Recruitment of the exosome to polyadenylated RNAs is mediated by the zinc finger protein ZFC3H1, which links the exosome cofactor MTR4 to PABPN1. This link was coined the poly(A) tail exosome targeting (PAXT) connection (also called the polysome protector complex, PPC) (15, 20). Overall, both PPD and the CBCN complex survey the integrity of RNAs to eliminate transcriptional noise, misprocessed and other potentially detrimental RNAs.

ARS2 directly interacts with the CBC to form a hub that allows the assembly of mutually exclusive complexes that dictate the fate of a transcript (13, 21, 24, 25). For instance, ARS2 interacts with PHAX or ALYREF to promote the nuclear export of properly processed snRNAs and mRNAs, respectively (21, 24-26). Alternatively, ARS2 recruits NEXT or PAXT to target RNAs for exosome-mediated degradation (13, 20, 27). In some

116 cases, ARS2 targets transcripts for degradation independently of NEXT or PPD/PAXT
117 (28, 29). These complex interconnections challenge efforts to uncover the degree of
118 independence or redundancy between nuclear RNA decay pathways. Nonetheless,
119 ARS2 clearly plays a central role in promoting the decay of a number of nuclear
120 transcripts.
121
122 Like their host counterparts, KSHV mRNAs are capped and polyadenylated, but most
123 KSHV genes are short and intronless (30, 31). Consequently, cellular RNA QC pathways
124 may degrade KSHV RNAs due to their similarity to PROMPTs. The essential
125 multifunctional KSHV ORF57 protein promotes viral transcript accumulation by increasing
126 nuclear RNA stability (32-45). We recently reported that viral transcripts are subject to
127 degradation by both PPD and an ARS2-dependent but NEXT-independent decay
128 pathway upon lytic reactivation of virus lacking ORF57 (29). Using pulse-chase assays
129 with an unstable form of the KSHV nuclear non-coding PAN RNA (PANΔENE), we further
130 showed that ORF57 preferentially protects viral transcripts from the ARS2-dependent
131 decay pathway (29). Interestingly, although viral transcripts succumb to PPD, ORF57
132 protection of PANΔENE from PPD was modest, suggesting the possibility that a subset
133 of viral transcripts undergo PPD-dependent degradation in the presence of ORF57 (29).
134 However, the role of PPD during viral infection with ORF57 expressing virus has not been
135 fully explored.
136
137 Here, we used RNAi to inactivate PPD and/or ARS2-dependent decay and monitored
138 their contributions to KSHV gene expression in the presence of ORF57 by RNA-seq at

24 hours after lytic reactivation. ARS2 depletion resulted in few changes in viral gene expression. However, PPD inactivation resulted in increased expression levels of several viral genes. Interestingly, the most upregulated transcripts were late transcripts that are otherwise expressed at ~48 hours after lytic reactivation. Our data suggest that PPD prevents the premature accumulation of late transcripts which presumably arise as a consequence of cryptic transcription. Notably, at their proper time of expression, PPD inactivation has no effect on viral late transcripts, and the host factor NRDE2 is needed for evasion of PPD. We conclude that KSHV exploits PPD to fine-tune the temporal expression of viral genes by dampening steady-state levels of prematurely transcribed late genes.

Results

PPD inactivation results in aberrant temporal expression of KSHV late genes

Our previous studies showed that viral RNAs were subject to both PPD and ARS2-mediated decay in the absence of ORF57 (29). ORF57 more potently protected viral transcripts from ARS2-mediated decay than from PPD, suggesting that viral transcripts succumb to PPD even in the presence of ORF57. To further characterize the role of these decay pathways during KSHV infection, we performed an RNA-seq experiment to monitor the levels of viral transcripts after siRNA depletion of ARS2, the PPD component PAPα/γ, or both simultaneously (dKD) in iSLK cells latently infected with the KSHV infectious clone BAC16 (iSLK WT) (46, 47)(Fig 1A). Efficiency of knockdown was

validated by western blot, qRT-PCR and/or loss of function assays (Fig 1B). Lytic reactivation was induced using doxycycline (dox) to promote expression of the dox-inducible RTA integrated into the iSLK host cell chromosomes and by the histone deacetylase inhibitor sodium butyrate (NaB). We prepared libraries from RNA harvested 24 hours post induction (hpi), and the samples were subjected to high-throughput sequencing (Fig 1A). Expression of several KSHV genes significantly increased in samples depleted of PAPα/γ and in the dKD compared to samples treated with a control siRNA. However, we observed minimal alterations in gene expression in the ARS2 knockdown samples, consistent with the idea that ARS2-mediated decay is inhibited by ORF57 (Fig 1C and Table S1). Surprisingly, the most upregulated genes (> 4-fold change) upon PAPα/γ depletion and in the dKD were late genes, 76% and 70% respectively (Fig 1D). Typically, these KSHV late genes are not expressed at ~24 hpi in these cells. These data suggest that KSHV exploits PAPα/γ to temporally control the expression of late genes.

PPD/PAXT targets KSHV late genes for degradation

Our RNA-seq data show that PAPα/γ depletion results in increased expression of late genes at 24 hpi and suggest that PPD controls the expression late genes that prematurely arise due to cryptic transcription. To validate these observations and extend the findings to additional PPD factors, we focused our attention on three KSHV late genes, ORF52, ORF75, and K8.1. These genes were selected because they have different structural features. ORF52 is a short transcript (395 base pairs (bp)) while ORF75 is a long

transcript (3890 bp). Both ORF52 and ORF75 are intronless, but K8.1 contains one intron. In spite of these structural differences, the expression of each gene increased upon PAPα/γ depletion at 24 hpi (Fig 2B, D and F). None were affected by ARS2 depletion alone. Similar results were obtained when the mRNA levels of these genes were monitored by qRT-PCR (Fig 2C, E and G). In principle, PAPα/γ knockdown may affect gene expression independent of PPD due to its function in 3´-end formation. To confirm the role of PPD, we tested whether depletion of PPD factors other than PAPα/γ caused a similar phenotype. We depleted cells of the unique PPD/PAXT factor ZFC3H1 or the exosome co-factor MTR4. Efficiency of knockdown was monitored by western blot, qRT-PCR and loss of function assays (Fig 2A). Consistent with PPD inactivation, depletion of ZFC3H1 or MTR4 also increased ORF75, ORF52 and K8.1 levels (Fig 2C, E and G). These data support the conclusion that PPD/PAXT suppresses KSHV late gene expression during the early stages of the virus lytic phase.

PPD regulates virus late gene expression independently of the viral transactivation factor ORF24

To elucidate the mechanism of late gene expression upregulation in the context of PPD inactivation, we first focused our attention on the requirements for late gene expression. In KSHV, transcription of late genes takes place after initiation of viral DNA replication, and their expression requires the action of several viral transactivation factors (vTF) (48-53). The viral TATA box-binding protein homolog, ORF24, is a KSHV transactivation factor that plays a critical role when the virus progresses from DNA replication to

208 expression of late genes. ORF24 binds to late gene promoters and recruits RNA
209 polymerase II (pol II) and other vTFs to the promoter region of late genes to induce their
210 expression. Because ORF24 mRNA levels were increased in cells depleted of PAPα/γ
211 and in the dKD at 24 hours post lytic reactivation (Fig 3A and 3B), it is possible that PPD
212 inactivation results in ORF24 upregulation which drives the increased expression of late
213 genes. In this case, the effects of PPD on other late transcripts would result from a
214 secondary effect of ORF24 upregulation. To determine whether the increased expression
215 of late genes at 24 hpi is due to an upregulation of ORF24 upon PPD inactivation, we
216 used iSLK cells transfected with a bacmid encoding the viral genome in which ORF24
217 contains a point mutation, R328A, that renders it inactive (51). ORF24^{R328A} maintains the
218 interaction with pol II but is unable to interact with other vTAs resulting in strongly impaired
219 expression of late genes (Fig 3C). If the up-regulation of late genes by PPD inactivation
220 is due to secondary effects of ORF24 upregulation, then the up-regulation will be
221 abrogated in the mutant virus. In contrast to this prediction, depletion of PPD components
222 PAPα/γ, MTR4 or ZFC3H1 resulted in increased mRNA levels of ORF52, ORF75 and
223 K8.1 in ORF24^{R328A} reactivated cells (Fig 3D, E and F). Thus, the role of PPD in late gene
224 expression at 24 hpi is independent of ORF24 transactivation. Moreover, these data are
225 consistent with a proposed role for PPD in the posttranscriptional inhibition of premature
226 late transcript accumulation.
227
228 **PPD control of late transcripts is restricted to early phases of reactivation but does**
229 **not affect genome replication or virus production in iSLK cells**
230

KSHV late genes are expressed after the initiation of viral genome replication (48-52), which occurs prior to 48 hpi in our iSLK WT cells. As PPD inactivation increases late gene expression at 24 hpi, we tested whether the expression of late genes at 48 and 72 hpi is also affected by PPD inactivation. Interestingly, at 48- or 72-hpi, PAPα/γ depletion had no effect on the expression levels of the late genes tested (Fig 4A, B and C). These data suggest that at the proper time of expression, KSHV late transcripts are able to avoid PPD-mediated degradation. They further support the model that PPD dampens premature expression of KSHV late genes.

Because of the aberrant timing of viral late gene expression, we investigated whether PPD inactivation affected virus fitness. To test genome replication, iSLK WT cells were depleted of PAPα/γ or ZFC3H1, and ORF57 DNA levels were monitored over time by qRT-PCR. Depletion of PAPα/γ or ZFC3H1 had no significant effect on the levels of viral genome replication at 48 hpi (Fig 4D). We next investigated whether PPD inactivation affects production of infectious virions. To test this, we collected media from iSLK WT cells at 0, 8, 12, 24, 48 and 72 hours after lytic reactivation and used it to infect HEK293 cells. Two days later, viral infection was analyzed by flow cytometry to detect the GFP expressed by BAC16. Most of the HEK293 cells infected with media collected from iSLK WT cells at 48 and 72 hpi were GFP positive (Fig 4E). Importantly, depletion of PAPα/γ or ZFC3H1 had no effect in the production of infectious virus as the percentage of GFP positive cells was similar to that of cells treated with a control siRNA (Fig 4E). These data suggest that the premature expression of late genes observed upon PPD inactivation does not dramatically perturb the virus life cycle in cultured cells.

254

255 **NRDE2 is needed for proper expression of late genes at 48 hours post lytic**
256 **reactivation**

257

258 To determine how late transcripts avoid degradation at their proper time of expression,
259 we centered our attention on the human nuclear RNAi-defective 2 (NRDE2) protein.
260 NRDE2 localizes to nuclear speckles where it forms a 1:1 complex with MTR4 to inhibit
261 its recruitment and RNA degradation (54). Given this protective activity, we hypothesized
262 that KSHV uses NRDE2 to protect late transcripts from degradation. Therefore, we
263 depleted cells of PAPα/γ, NRDE2 (Fig 5A) or both simultaneously and measured
264 expression levels of late transcripts by qRT-PCR at 24 hpi (Fig 5B) or 48 hpi (Fig 5C). As
265 expected, PAPα/γ depletion resulted in increased expression levels of late genes at 24
266 hpi but no effect at 48 hpi (Fig 5B and C) (green bars). In contrast, NRDE2 depletion
267 caused a reduction in expression levels of all late transcripts at 48 hpi but had no effect
268 at 24 hpi (Fig 5B and C) (orange bars) suggesting that NRDE2 protects KSHV late
269 transcripts from PPD-mediated degradation at 48 hpi. Importantly, co-depletion of PAPα/γ
270 and NRDE2 restored late transcripts levels to that of control siRNA treated cells (Fig 5C)
271 (blue bars). We conclude that after viral genome replication, the host NRDE2 protects
272 KSHV RNAs from PPD.

273

274

275

276

Discussion

KSHV transcripts are subject to degradation by at least two host-mediated nuclear RNA decay pathways, PPD and an ARS2-dependent decay pathway (29). KSHV ORF57 increases viral transcript stability by protecting RNAs from ARS2-dependent decay (29). Our work here suggests that KSHV uses PPD to post-transcriptionally control the premature accumulation of late transcripts during the early stages of the viral lytic phase. In the context of PPD inactivation, late transcripts aberrantly accumulate at 24 hpi (Fig 1 and 2), but the premature production of late transcripts does not require functional ORF24. Therefore, the transcripts do not accumulate as a secondary consequence of the up-regulation of the late gene inducer ORF24 (Fig 3). Presumably, the open chromatin and high transcription of the viral genome during early lytic phase allows low-level cryptic transcription of late genes (Fig 6A). The transcripts are eliminated by PPD, so no proteins are produced. At their proper time of expression, late transcripts evade PPD by an NRDE2-dependent mechanism (Fig 5). Thus, we propose that KSHV fine-tunes temporal expression of its genes using a specific host RNA quality control pathway.

Increasing evidence shows that RNA decay pathways play a critical role in controlling viral infection (29, 55-57). The nuclear RNA decay factors, MTR4 and ZCCHC7, translocate to the cytoplasm where they promote exosome-mediated degradation of viral transcripts of multiple RNA virus (55). In the case of KSHV, the ORF57 protein protects viral transcript from ARS2-dependent decay by preventing MTR4 recruitment (29). In these examples, the viruses must circumvent the RNA QC machinery to properly express

its genes. Here we propose that the virus hijacks PPD activity to fine-tune the temporal expression of its genes. That is, KSHV allows PPD to degrade late transcripts that arise as a consequence of cryptic transcription at 24 hpi (Fig 2 and 6A). However, at the appropriate time of expression, KSHV blocks PPD so late genes are expressed (Fig 4A-C). The long co-evolution of herpesviruses with their specific hosts has selected for sophisticated host-pathogen interactions. These contrasting interactions with the host RNA QC pathways represent intriguing examples of virus-host co-evolution that ensures KSHV expresses its genes in a precise temporal manner.

Our observations also contribute to the understanding of the distinctions between host PPD, PAXT and ARS2-mediated decay processes. While it seems likely that PPD and PAXT represent the same pathway, it has been reported that ARS2 is involved in PAXT recruitment to unstable transcripts (20). However, in the context of KSHV infection, PPD and an ARS2-mediated decay pathway appear to be independent pathways. For example, simultaneous depletion of PAPα/γ and ARS2 resulted in greater stabilization of viral transcripts than depletion of either alone during iSLK-ΔORF57 reactivation (29). Furthermore, we show that depletion of PAPα/γ enhances specific viral genes, while ARS2 depletion has little effect (Figs 1 and 2). Importantly, we show that depletion of ZFC3H1, a PAXT component, mimics PAPα/γ depletion as the same group of viral genes are upregulated (Fig 2). Overall, these data suggest that PPD and PAXT represent the same process, but ARS2 is not absolutely required for PPD/PAXT-mediated decay. However, more work is needed to completely define the overlap and independence of these RNA QC pathways.

PPD inactivation results in the aberrant temporal expression of KSHV late genes. However, this atypical expression of late genes does not affect viral genome replication or production of infectious virions in our iSLK cells (Fig 4D & E). Several reasons may explain this unexpected result. Even though PAP knockdown increases late gene expression levels relative to cells treated with a control siRNA, the expression levels reached may not be high enough to affect viral fitness. Indeed, expression of late genes at 48 or 72 hpi is considerably higher than at 24 hpi (Fig 4A-C). Consequently, the levels of late genes reached at 24 hpi may not be sufficient to disrupt viral physiology in iSLK cells. Another possibility is that the virus uses PPD to keep expression levels of late genes low during early phases of lytic infection as these may elicit an immune response in an infected organism. Indeed, circulating anti-K8.1 antibodies detected in Kaposi's sarcoma patients support that this PPD-restricted gene elicits an immune response (58-60). If the role of PPD is to keep potentially immunogenic genes low, we would miss this phenotype in a cell culture system.

Late transcripts evade PPD during late phases of replication, but the mechanism of PPD evasion is not completely understood. Our data show that the host factor NRDE2 is required for evasion of PPD during late infection (Fig 5). NRDE2 function is linked to its residence in nuclear speckles, where it interacts with MTR4 to inhibit its activity thereby protecting speckle-associated mRNAs (54). As expression of KSHV late genes occurs at the onset of viral genome replication, we speculate that NRDE2 re-localizes to replication compartments (Fig 6B). When this occurs, NRDE2 interacts with MTR4 preventing the recruitment of the nuclear exosome to viral transcripts. Consequently, late transcripts

evade PPD and are properly expressed. Supporting this idea, HSV1 replication compartments coalesce with nuclear speckles (61), but whether this occurs in KSHV has yet to be tested.

Additional factors may contribute to protection of late transcripts from PPD during late phases of KSHV reactivation. For example, expression of KSHV late genes requires the action of several viral transactivation factors (48-52). ORF24 is essential to recruit RNA pol II and other viral transactivation factors to late gene promoters (51). In principle, ORF24-induced transcription may promote the co-transcriptional recruitment of factors that protect transcripts from degradation. Evasion and exploitation of nuclear RNA decay pathways by KSHV is only beginning to be understood. Further experimentation is needed to substantiate the role of NRDE2 and identify other factors involved in these processes.

Materials and Methods

RNA-seq: library preparation

iSLK WT cells were transfected with a non-targeting control siRNA or a two-siRNA pool targeting PAPα and PAPγ (PAPα/γ), ARS2 or both PAPα/γ and ARS2 combined (dKD) using the concentrations specified in the siRNA transfection section. Total RNA was harvested three days after siRNA transfection and 24 hours post lytic reactivation. One

µg of intact total RNA per condition was used to make stranded mRNA-seq libraries with the Stranded mRNA-Seq kit (KAPA Biosystems) as per manufacturer's protocol. The strand-specific single-end RNA-sequencing was performed using Illumina HiSeq2500.

RNA-seq analysis

The qualities of sequencing reads were evaluated using NGS QC Toolkit (v2.3.3) (62) and high-quality reads were extracted. The human reference genome sequence and gene annotation data, hg19, were downloaded from Illumina iGenomes (https://support.illumina.com/sequencing/sequencing_software/igenome.html). The viral genome was downloaded from NCBI GenBank (https://www.ncbi.nlm.nih.gov/nuccore/GQ994935.1). The qualities of RNA-sequencing libraries were estimated by mapping the reads onto human transcript and ribosomal RNA sequences (Ensembl release 89) using Bowtie (v2.2.9) (63). STAR (v2.5.2b) (53) was employed to align the reads onto the human and viral genomes, Picard (v1.140) (https://broadinstitute.github.io/picard/) was employed to sort the alignments, and HTSeq Python package (64) was employed to count reverse-stranded reads per gene. DESeq2 R Bioconductor package (65) was used to normalize read counts and identify differentially expressed (DE) genes. The resulting gene expression analyses are given in Supplementary Tables S1 for viral genes exclusively and S2 for human plus viral genes. The enrichment of DE genes to pathways and GOs were calculated by Fisher's exact test in R statistical package. Genome coverages were calculated using SAMtools (v0.1.19) (66), BEDTools (v2.26) (67), and bedGraphToBigWig

(https://genome.ucsc.edu/index.html). The heatmap was generated using Morpheus from the Broad Institute (https://software.broadinstitute.org/morpheus/).

The data discussed in this publication have been deposited in NCBI's Gene Expression Omnibus (68) and are accessible through GEO Series accession number GSE144747 (https://www.ncbi.nlm.nih.gov/geo/query/acc.cgi?acc=GSE144747).

Cell Culture

iSLK cells were grown at 37°C with 5% CO_2 in DMEM (Sigma) supplemented with 10% Tet-Free fetal bovine serum (FBS, Atlanta Biologicals), 1x penicillin-streptomycin (Sigma), and 2 mM L-glutamine (Fisher). iSLK WT cells were grown in the presence of 0.1 mg/mL G418 (Fisher), 1 µg/mL puromycin (Sigma) and 50 µg/mL hygromycin. iSLK-ORF24^{R328A} cells (gift from Dr. Britt Glaunsinger, University of California Berkeley) were grown under the same conditions, except 200 µg/mL of hygromycin was used.

siRNA Transfections

iSLK cells were transfected with 20 or 40 nM siRNA (Silencer Select, ThermoFisher) using RNAiMAX transfection reagent (Invitrogen) per manufacturer's instruction. Specifically, we used final concentrations of 40 nM siRNAs for ZFC3H1, MTR4 and NRDE2 and 20 nM siRNAs ARS2. For PAPα/γ, we used 20 nM each of siRNAs that target PAPα or PAPγ for a total of 40 nM siRNA. Twenty-four hours after siRNA transfection, cells were split into new plates and allowed to grow for another 24 hours, after which

416 doxycycline and NaB was added to induce lytic reactivation. Thus, total RNA was
417 harvested 72 hours post siRNA transfection and 24 hours post lytic reactivation.
418 Nontargeting control, PAPα/γ, ZC3H1 and MTR4 siRNAs are the same as previously
419 used (29). NRDE2 siRNAs are: 5' GGUGUUGUUUGAUGAUAUUtt 3' (s30063) and 5'
420 GUUUAGUACCUUUUCGAUAtt 3' (s30064).
421

422 **Quantitative RT-PCR**

423

424 RNA was harvested using TRI reagent (Molecular Research Center, Inc.) according to
425 the manufacturer's protocol. Following extraction, RNA was treated with RQ1 DNase
426 (Promega). Oligo dT_{20} was used to prime cDNA synthesis with MuLV reverse
427 transcriptase (New England Biolabs). Real-time reactions used iTaq Universal SYBR
428 Green Supermix (Biorad). Primers are listed in Table S3.
429

430 **KSHV Reactivation and Infection**

431

432 Lytic reactivation of iSLK derived cells was achieved by adding doxycycline (1 μg/ml) and
433 NaB (1mM). Tissue culture supernatants from iSLK WT cells were collected at 0, 8, 12,
434 24, 48 and 72 hpi, centrifuged for 5 min at 1000 x g and passed through a 0.45 um filter.
435 Polybrene was added (8 μg/mL final concentration), and 300 μL were applied to HEK293
436 cells grown in a 12-well plate. Cells were centrifuged for 45 min at 30°C and then
437 incubated in 5% CO_2 at 37°C for 2 hours. After this, media was replaced and cells were
438 analyzed by flow cytometry 24 hours later.

Western Blotting

Cells were lysed in buffer containing 100 mM NaCl, 50 mM Tris-HCl pH 7.4, 1% Triton X-100, 1X Protease Inhibitor cocktail (PIC) (Calbiochem) and 250 μM PMSF. Proteins were resolved by SDS-PAGE and analyzed by western blot using standard procedures. Antibodies used are rabbit polyclonal anti-ARS2 (Abcam, ab192999), rabbit polyclonal anti-MTR4 (Abcam, Ab70551), rabbit polyclonal anti-NRDE2 (Proteintech, 24968) and mouse monoclonal anti-Actin (Abcam, ab6276). Quantitative westerns were performed using infrared detection with an Odyssey Fc and quantification was performed using ImageStudio software (LI-COR Biosciences).

Acknowledgements

We thank Anna Scarborough and Juliana Flaherty for critical review of this manuscript. We thank Dr. Divya Nandakumar, Jennifer Blancas and Dr. Britt Glaunsinger (UC Berkeley) for the iSLK ORF24^{R328A} cells. We thank Spencer Barnes (UTSW) for GEO submission. The work was supported by NIH/NIAID R01 AI123165 (to N.K.C.), the Welch Foundation I-1915-20170325 (to N.K.C) and Cancer Prevention and Research Institute of Texas RP150596 (to the Bioinformatics Core Facility, UTSW).

Figure Legends

Fig 1. PPD inactivation affects the temporal expression of KSHV late genes. (A) Diagram of the RNA-seq experiment. iSLK WT cells were transfected with a non-targeting control siRNA or a two-siRNA pool targeting PAPα/γ, ARS2, or both PAPα/γ and ARS2 combined (dKD). Total RNA was harvested three days after siRNA transfection and 24 hours after lytic reactivation. Stranded mRNA-seq libraries were prepared and sequenced. (B) Efficiency of knockdown of PAPα, PAPγ, and ARS2 in iSLK WT cells. Due to the lack of robust antibodies, PAPα and PAPγ knockdown efficiency was determined by qRT-PCR. Bar graphs show PAPα and PAPγ mRNA levels in iSLK WT cells treated with siRNAs targeting PAPα and PAPγ. Because RNA knockdown does not necessarily correlate with protein loss, we assayed for loss of functional activity. To do so, we measured the RNA levels of a known PPD target, NEAT1, under the same conditions used for RNA-seq. Bar graph shows NEAT1 levels determined by qRT-PCR in iSLK WT cells depleted of PAPα/γ. Values are displayed relative to siCtrl after normalization to the 18S rRNA level. All values are averages, and the error bars are standard deviations (n = 3). ARS2 knockdown efficiency was determined by quantitative western blot. Actin serves as loading control. (C) Heatmap showing the log2 fold change (FC) relative to siCtrl for all KSHV genes in samples depleted of PAPα/γ, ARS2 or dKD. Genes are arranged in increasing log2 FC order based on PAPα/γ, where red represents maximum fold change and blue represents Log2 FC <1.5. (D) Pie charts showing the distribution of upregulated (>4-fold) KSHV genes in PAPα/γ (top) and dKD (bottom) according to their phase of expression (30).

Fig 2. KSHV late transcripts are degraded by PPD/PAXT. (A) Efficiency of knockdown of ZFC3H1 and MTR4 in iSLK WT cells. Bar graphs show ZFC3H1 and NEAT1 mRNA levels in iSLK WT cells treated with ZFC3H1 siRNAs. Increased levels of NEAT1 indicate that PPD was effectively inactivated upon ZFC3H1 depletion. MTR4 knockdown efficiency was determined by quantitative western blot. Actin serves as loading control. (*) nonspecific band. (B, D and F) Integrative genome viewer (IGV) browser screenshots showing ORF75 (B), ORF52 (D) and K8.1 (F) reads in samples depleted of PAPα/γ, ARS2 or dKD. Each condition is depicted at the same scale. (C, E and G) Bar graphs showing relative ORF75 (C), ORF52 (E) and K8.1 (G) mRNA levels in iSLK WT cells depleted of PAPα/γ (green), ARS2 (orange), dKD (red), ZFC3H1 (purple) and MTR4 (light blue). Total RNA was harvested 24 hpi and analyzed by qRT-PCR. Values are displayed relative to siCtrl after normalization to the 18S rRNA level. All values are averages, and the error bars are standard deviations (n = 3). *P* values were determined by two-tailed unpaired Student's *t* test: * < 0.05; ** < 0.01; *** < 0.001.

Fig 3. PPD upregulation of late genes is independent of ORF24. (A) IGV browser screenshot showing ORF24 reads in samples depleted of PAPα/γ, ARS2 or dKD. (B) Bar graphs showing relative ORF24 mRNA levels in iSLK cells depleted of PAPα/γ (green), ARS2 (orange) and dKD (red). (C) Bar graphs showing relative ORF52, ORF75 and K8.1 mRNA level in iSLK WT (gray) and iSLK ORF24^{R328A} (white) cells at 48 hpi. (D, E and F) Bar graphs showing relative ORF52 (D), ORF75 (E) and K8.1 (F) mRNA levels in iSLK ORF24^{R328A} cells depleted of PAPα/γ (green), ARS2 (orange), dKD (red), ZFC3H1

(purple) and MTR4 (light blue). Total RNA was harvested 24 hpi and analyzed by qRT-PCR. Values are displayed relative to siCtrl after normalization to the 18S rRNA level. All values are averages, and the error bars are standard deviations (n = 3). *P* values were determined by two-tailed unpaired Student's *t* test: * < 0.05; ** < 0.01; *** < 0.001.

Fig 4. KSHV late transcripts evade PPD degradation at their proper time of expression (A, B and C) Bar graphs showing relative ORF75 (A), ORF52 (B) and K8.1 (C) mRNA levels in iSLK WT cells treated with siRNAs targeting PAPα/γ (green) or a control siRNA (gray). Total RNA was harvested at 24, 48 and 72 hpi. Values were calculated relative to siCtrl at 24 hpi (gray) and normalized to the 18S rRNA level. Note that the data are plotted on a log scale due to the strong up-regulation of late genes after 48 hpi. (D) Bar graphs showing relative ORF57 DNA levels in iSLK WT cells depleted of PAPα/γ (green) or ZFC3H1 (purple). DNA was harvested at 0, 12, 24 and 48 hpi. Values were calculated relative to siCtrl (gray) at 0 hpi. (E) Bar graph of flow cytometry analysis showing percentage of GFP-positive HEK293 cells infected with supernatants collected from iSLK WT cells at 0, 8, 12, 24, 48 and 72 hpi. All values are averages, and the error bars are standard deviations (n = 3). *P* values were determined by Student's *t* test: * < 0.05; ** < 0.01; *** < 0.0001.

Fig 5. NRDE2 protects viral late transcripts from degradation. (A) NRDE2 knockdown efficiency was determined by quantitative western blot. Actin serves as loading control. (*) nonspecific band. (B and C) Bar graphs showing relative ORF75, ORF52 and K8.1 mRNA levels at 24 (B) and 48 (C) hpi in iSLK WT depleted of PAPα/γ (green), NRDE2

(orange) and PAPα/γ and NRDE2 combined (blue). Total RNA was harvested 24 or 48 hpi and analyzed by qRT-PCR. Values are displayed relative to siCtrl after normalization to the 18S rRNA level. All values are averages, and the error bars are standard deviations (n = 3). *P* values were determined by two-tailed unpaired Student's *t* test: * < 0.05; ** < 0.01; *** < 0.001.

Fig 6. Model of PPD regulation of KSHV late genes. (A) KSHV late genes are cryptically transcribed at 24 hpi, but the transcripts do not accumulate due to PPD. (B) At 48 hpi, KSHV late transcripts evade PPD and accumulate at high levels. We speculate that KSHV replication compartments coalesce with nuclear speckles where NRDE2 protects viral transcripts from PPD degradation by sequestering MTR4.

Table S1. Differential expression of KSHV genes. This spreadsheet contains the expression levels of all KSHV genes in samples depleted of PAPα/γ, ARS2 and dKD relative to siCtrl.

Table S2. Differential expression of human and KSHV genes. This spreadsheet contains the expression levels of human and KSHV genes in samples depleted of PAPα/γ, ARS2 and dKD relative to siCtrl.

Table S3. Primers used in this study. Target, sequence, and primer number (ID) for all PCR primers used herein.

554

555 **References**

556

557 1. Dittmer DP, Damania B. 2016. Kaposi sarcoma-associated herpesvirus:
558 immunobiology, oncogenesis, and therapy. J Clin Invest 126:3165-75.
559 2. Kaplan LD. 2013. Human herpesvirus-8: Kaposi sarcoma, multicentric Castleman
560 disease, and primary effusion lymphoma. Hematology Am Soc Hematol Educ
561 Program 2013:103-8.
562 3. Ruocco E, Ruocco V, Tornesello ML, Gambardella A, Wolf R, Buonaguro FM.
563 2013. Kaposi's sarcoma: etiology and pathogenesis, inducing factors, causal
564 associations, and treatments: facts and controversies. Clin Dermatol 31:413-422.
565 4. Staudt MR, Dittmer DP. 2003. Viral latent proteins as targets for Kaposi's sarcoma
566 and Kaposi's sarcoma-associated herpesvirus (KSHV/HHV-8) induced lymphoma.
567 Curr Drug Targets Infect Disord 3:129-35.
568 5. Bellare P, Ganem D. 2009. Regulation of KSHV lytic switch protein expression by
569 a virus-encoded microRNA: an evolutionary adaptation that fine-tunes lytic
570 reactivation. Cell Host Microbe 6:570-5.
571 6. Deng H, Liang Y, Sun R. 2007. Regulation of KSHV lytic gene expression. Curr
572 Top Microbiol Immunol 312:157-83.
573 7. Staudt MR, Dittmer DP. 2007. The Rta/Orf50 transactivator proteins of the gamma-
574 herpesviridae. Curr Top Microbiol Immunol 312:71-100.
575 8. Bresson S, Tollervey D. 2018. Surveillance-ready transcription: nuclear RNA
576 decay as a default fate. Open Biol 8.

9. Doma MK, Parker R. 2007. RNA quality control in eukaryotes. Cell 131:660-8.

10. Fasken MB, Corbett AH. 2009. Mechanisms of nuclear mRNA quality control. RNA Biol 6:237-41.

11. Garland W, Jensen TH. 2019. Nuclear sorting of RNA. Wiley Interdiscip Rev RNA doi:10.1002/wrna.1572:e1572.

12. Maquat LE, Kiledjian M. 2008. RNA turnover in eukaryotes: analysis of specialized and quality control RNA decay pathways. Preface. Methods Enzymol 449:xvii-xviii.

13. Andersen PR, Domanski M, Kristiansen MS, Storvall H, Ntini E, Verheggen C, Schein A, Bunkenborg J, Poser I, Hallais M, Sandberg R, Hyman A, LaCava J, Rout MP, Andersen JS, Bertrand E, Jensen TH. 2013. The human cap-binding complex is functionally connected to the nuclear RNA exosome. Nat Struct Mol Biol 20:1367-76.

14. Bresson SM, Hunter OV, Hunter AC, Conrad NK. 2015. Canonical Poly(A) Polymerase Activity Promotes the Decay of a Wide Variety of Mammalian Nuclear RNAs. PLoS Genet 11:e1005610.

15. Ogami K, Richard P, Chen Y, Hoque M, Li W, Moresco JJ, Yates JR, 3rd, Tian B, Manley JL. 2017. An Mtr4/ZFC3H1 complex facilitates turnover of unstable nuclear RNAs to prevent their cytoplasmic transport and global translational repression. Genes Dev 31:1257-1271.

16. Flynn RA, Almada AE, Zamudio JR, Sharp PA. 2011. Antisense RNA polymerase II divergent transcripts are P-TEFb dependent and substrates for the RNA exosome. Proc Natl Acad Sci U S A 108:10460-5.

17. Preker P, Almvig K, Christensen MS, Valen E, Mapendano CK, Sandelin A, Jensen TH. 2011. PROMoter uPstream Transcripts share characteristics with mRNAs and are produced upstream of all three major types of mammalian promoters. Nucleic Acids Res 39:7179-93.

18. Preker P, Nielsen J, Kammler S, Lykke-Andersen S, Christensen MS, Mapendano CK, Schierup MH, Jensen TH. 2008. RNA exosome depletion reveals transcription upstream of active human promoters. Science 322:1851-4.

19. Bresson SM, Conrad NK. 2013. The human nuclear poly(a)-binding protein promotes RNA hyperadenylation and decay. PLoS Genet 9:e1003893.

20. Meola N, Domanski M, Karadoulama E, Chen Y, Gentil C, Pultz D, Vitting-Seerup K, Lykke-Andersen S, Andersen JS, Sandelin A, Jensen TH. 2016. Identification of a Nuclear Exosome Decay Pathway for Processed Transcripts. Mol Cell 64:520-533.

21. Lubas M, Christensen MS, Kristiansen MS, Domanski M, Falkenby LG, Lykke-Andersen S, Andersen JS, Dziembowski A, Jensen TH. 2011. Interaction profiling identifies the human nuclear exosome targeting complex. Mol Cell 43:624-37.

22. Lingaraju M, Johnsen D, Schlundt A, Langer LM, Basquin J, Sattler M, Heick Jensen T, Falk S, Conti E. 2019. The MTR4 helicase recruits nuclear adaptors of the human RNA exosome using distinct arch-interacting motifs. Nat Commun 10:3393.

23. Beaulieu YB, Kleinman CL, Landry-Voyer AM, Majewski J, Bachand F. 2012. Polyadenylation-dependent control of long noncoding RNA expression by the poly(A)-binding protein nuclear 1. PLoS Genet 8:e1003078.

622 24. Giacometti S, Benbahouche NEH, Domanski M, Robert MC, Meola N, Lubas M,
623 Bukenborg J, Andersen JS, Schulze WM, Verheggen C, Kudla G, Jensen TH,
624 Bertrand E. 2017. Mutually Exclusive CBC-Containing Complexes Contribute to
625 RNA Fate. Cell Rep 18:2635-2650.
626 25. Schulze WM, Stein F, Rettel M, Nanao M, Cusack S. 2018. Structural analysis of
627 human ARS2 as a platform for co-transcriptional RNA sorting. Nat Commun
628 9:1701.
629 26. Hallais M, Pontvianne F, Andersen PR, Clerici M, Lener D, Benbahouche Nel H,
630 Gostan T, Vandermoere F, Robert MC, Cusack S, Verheggen C, Jensen TH,
631 Bertrand E. 2013. CBC-ARS2 stimulates 3'-end maturation of multiple RNA
632 families and favors cap-proximal processing. Nat Struct Mol Biol 20:1358-66.
633 27. Iasillo C, Schmid M, Yahia Y, Maqbool MA, Descostes N, Karadoulama E,
634 Bertrand E, Andrau JC, Jensen TH. 2017. ARS2 is a general suppressor of
635 pervasive transcription. Nucleic Acids Res 45:10229-10241.
636 28. Fan J, Kuai B, Wu G, Wu X, Chi B, Wang L, Wang K, Shi Z, Zhang H, Chen S, He
637 Z, Wang S, Zhou Z, Li G, Cheng H. 2017. Exosome cofactor hMTR4 competes
638 with export adaptor ALYREF to ensure balanced nuclear RNA pools for
639 degradation and export. EMBO J 36:2870-2886.
640 29. Ruiz JC, Hunter OV, Conrad NK. 2019. Kaposi's sarcoma-associated herpesvirus
641 ORF57 protein protects viral transcripts from specific nuclear RNA decay pathways
642 by preventing hMTR4 recruitment. PLoS Pathog 15:e1007596.
643 30. Arias C, Weisburd B, Stern-Ginossar N, Mercier A, Madrid AS, Bellare P, Holdorf
644 M, Weissman JS, Ganem D. 2014. KSHV 2.0: a comprehensive annotation of the

645 Kaposi's sarcoma-associated herpesvirus genome using next-generation
646 sequencing reveals novel genomic and functional features. PLoS Pathog
647 10:e1003847.
648 31. Zheng ZM. 2003. Split genes and their expression in Kaposi's sarcoma-associated
649 herpesvirus. Rev Med Virol 13:173-84.
650 32. Duan W, Wang S, Liu S, Wood C. 2001. Characterization of Kaposi's sarcoma-
651 associated herpesvirus/human herpesvirus-8 ORF57 promoter. Arch Virol
652 146:403-13.
653 33. Han Z, Swaminathan S. 2006. Kaposi's sarcoma-associated herpesvirus lytic gene
654 ORF57 is essential for infectious virion production. J Virol 80:5251-60.
655 34. Majerciak V, Pripuzova N, McCoy JP, Gao SJ, Zheng ZM. 2007. Targeted
656 disruption of Kaposi's sarcoma-associated herpesvirus ORF57 in the viral genome
657 is detrimental for the expression of ORF59, K8alpha, and K8.1 and the production
658 of infectious virus. J Virol 81:1062-71.
659 35. Majerciak V, Yamanegi K, Allemand E, Kruhlak M, Krainer AR, Zheng ZM. 2008.
660 Kaposi's sarcoma-associated herpesvirus ORF57 functions as a viral splicing
661 factor and promotes expression of intron-containing viral lytic genes in
662 spliceosome-mediated RNA splicing. J Virol 82:2792-801.
663 36. Malik P, Blackbourn DJ, Cheng MF, Hayward GS, Clements JB. 2004. Functional
664 co-operation between the Kaposi's sarcoma-associated herpesvirus ORF57 and
665 ORF50 regulatory proteins. J Gen Virol 85:2155-66.

666 37. Malik P, Schirmer EC. 2006. The Kaposi's sarcoma-associated herpesvirus
667 ORF57 protein: a pleurotropic regulator of gene expression. Biochem Soc Trans
668 34:705-10.
669 38. Palmeri D, Spadavecchia S, Carroll KD, Lukac DM. 2007. Promoter- and cell-
670 specific transcriptional transactivation by the Kaposi's sarcoma-associated
671 herpesvirus ORF57/Mta protein. J Virol 81:13299-314.
672 39. Sei E, Conrad NK. 2011. Delineation of a core RNA element required for Kaposi's
673 sarcoma-associated herpesvirus ORF57 binding and activity. Virology 419:107-16.
674 40. Conrad NK. 2016. New insights into the expression and functions of the Kaposi's
675 sarcoma-associated herpesvirus long noncoding PAN RNA. Virus Res 212:53-63.
676 41. Kirshner JR, Lukac DM, Chang J, Ganem D. 2000. Kaposi's sarcoma-associated
677 herpesvirus open reading frame 57 encodes a posttranscriptional regulator with
678 multiple distinct activities. J Virol 74:3586-97.
679 42. Majerciak V, Pripuzova N, Chan C, Temkin N, Specht SI, Zheng ZM. 2015. Stability
680 of structured Kaposi's sarcoma-associated herpesvirus ORF57 protein is regulated
681 by protein phosphorylation and homodimerization. J Virol 89:3256-74.
682 43. Massimelli MJ, Kang JG, Majerciak V, Le SY, Liewehr DJ, Steinberg SM, Zheng
683 ZM. 2011. Stability of a long noncoding viral RNA depends on a 9-nt core element
684 at the RNA 5' end to interact with viral ORF57 and cellular PABPC1. Int J Biol Sci
685 7:1145-60.
686 44. Nekorchuk M, Han Z, Hsieh TT, Swaminathan S. 2007. Kaposi's sarcoma-
687 associated herpesvirus ORF57 protein enhances mRNA accumulation
688 independently of effects on nuclear RNA export. J Virol 81:9990-8.

689 45. Sahin BB, Patel D, Conrad NK. 2010. Kaposi's sarcoma-associated herpesvirus
690 ORF57 protein binds and protects a nuclear noncoding RNA from cellular RNA
691 decay pathways. PLoS Pathog 6:e1000799.
692 46. Brulois KF, Chang H, Lee AS, Ensser A, Wong LY, Toth Z, Lee SH, Lee HR,
693 Myoung J, Ganem D, Oh TK, Kim JF, Gao SJ, Jung JU. 2012. Construction and
694 manipulation of a new Kaposi's sarcoma-associated herpesvirus bacterial artificial
695 chromosome clone. J Virol 86:9708-20.
696 47. Myoung J, Ganem D. 2011. Generation of a doxycycline-inducible KSHV producer
697 cell line of endothelial origin: maintenance of tight latency with efficient reactivation
698 upon induction. J Virol Methods 174:12-21.
699 48. Butnaru M, Gaglia MM. 2019. The Kaposi's Sarcoma-Associated Herpesvirus
700 Protein ORF42 Is Required for Efficient Virion Production and Expression of Viral
701 Proteins. Viruses 11.
702 49. Castaneda AF, Glaunsinger BA. 2019. The Interaction between ORF18 and
703 ORF30 Is Required for Late Gene Expression in Kaposi's Sarcoma-Associated
704 Herpesvirus. J Virol 93.
705 50. Chang J, Ganem D. 2000. On the control of late gene expression in Kaposi's
706 sarcoma-associated herpesvirus (human herpesvirus-8). J Gen Virol 81:2039-47.
707 51. Davis ZH, Hesser CR, Park J, Glaunsinger BA. 2016. Interaction between ORF24
708 and ORF34 in the Kaposi's Sarcoma-Associated Herpesvirus Late Gene
709 Transcription Factor Complex Is Essential for Viral Late Gene Expression. J Virol
710 90:599-604.

711 52. Nishimura M, Watanabe T, Yagi S, Yamanaka T, Fujimuro M. 2017. Kaposi's
712 sarcoma-associated herpesvirus ORF34 is essential for late gene expression and
713 virus production. Sci Rep 7:329.
714 53. Brulois K, Wong LY, Lee HR, Sivadas P, Ensser A, Feng P, Gao SJ, Toth Z, Jung
715 JU. 2015. Association of Kaposi's Sarcoma-Associated Herpesvirus ORF31 with
716 ORF34 and ORF24 Is Critical for Late Gene Expression. J Virol 89:6148-54.
717 54. Wang J, Chen J, Wu G, Zhang H, Du X, Chen S, Zhang L, Wang K, Fan J, Gao S,
718 Wu X, Zhang S, Kuai B, Zhao P, Chi B, Wang L, Li G, Wong CCL, Zhou Y, Li J,
719 Yun C, Cheng H. 2019. NRDE2 negatively regulates exosome functions by
720 inhibiting MTR4 recruitment and exosome interaction. Genes Dev 33:536-549.
721 55. Molleston JM, Sabin LR, Moy RH, Menghani SV, Rausch K, Gordesky-Gold B,
722 Hopkins KC, Zhou R, Jensen TH, Wilusz JE, Cherry S. 2016. A conserved virus-
723 induced cytoplasmic TRAMP-like complex recruits the exosome to target viral RNA
724 for degradation. Genes Dev 30:1658-70.
725 56. Sabin LR, Zhou R, Gruber JJ, Lukinova N, Bambina S, Berman A, Lau CK,
726 Thompson CB, Cherry S. 2009. Ars2 regulates both miRNA- and siRNA-
727 dependent silencing and suppresses RNA virus infection in Drosophila. Cell
728 138:340-51.
729 57. Sokoloski KJ, Wilusz CJ, Wilusz J. 2006. Viruses: overturning RNA turnover. RNA
730 Biol 3:140-4.
731 58. Engels EA, Clark E, Aledort LM, Goedert JJ, Whitby D. 2002. Kaposi's sarcoma-
732 associated herpesvirus infection in elderly Jews and non-Jews from New York City.
733 Int J Epidemiol 31:946-50.

734 59. Li M, MacKey J, Czajak SC, Desrosiers RC, Lackner AA, Jung JU. 1999.
735 Identification and characterization of Kaposi's sarcoma-associated herpesvirus
736 K8.1 virion glycoprotein. J Virol 73:1341-9.
737 60. Wilkinson J, Cope A, Gill J, Bourboulia D, Hayes P, Imami N, Kubo T, Marcelin A,
738 Calvez V, Weiss R, Gazzard B, Boshoff C, Gotch F. 2002. Identification of Kaposi's
739 sarcoma-associated herpesvirus (KSHV)-specific cytotoxic T-lymphocyte epitopes
740 and evaluation of reconstitution of KSHV-specific responses in human
741 immunodeficiency virus type 1-Infected patients receiving highly active
742 antiretroviral therapy. J Virol 76:2634-40.
743 61. Chang L, Godinez WJ, Kim IH, Tektonidis M, de Lanerolle P, Eils R, Rohr K, Knipe
744 DM. 2011. Herpesviral replication compartments move and coalesce at nuclear
745 speckles to enhance export of viral late mRNA. Proc Natl Acad Sci U S A
746 108:E136-44.
747 62. Patel RK, Jain M. 2012. NGS QC Toolkit: a toolkit for quality control of next
748 generation sequencing data. PLoS One 7:e30619.
749 63. Langmead B, Salzberg SL. 2012. Fast gapped-read alignment with Bowtie 2. Nat
750 Methods 9:357-9.
751 64. Anders S, Pyl PT, Huber W. 2015. HTSeq--a Python framework to work with high-
752 throughput sequencing data. Bioinformatics 31:166-9.
753 65. Gentleman RC, Carey VJ, Bates DM, Bolstad B, Dettling M, Dudoit S, Ellis B,
754 Gautier L, Ge Y, Gentry J, Hornik K, Hothorn T, Huber W, Iacus S, Irizarry R,
755 Leisch F, Li C, Maechler M, Rossini AJ, Sawitzki G, Smith C, Smyth G, Tierney L,

Yang JY, Zhang J. 2004. Bioconductor: open software development for computational biology and bioinformatics. Genome Biol 5:R80.

66. Li H, Handsaker B, Wysoker A, Fennell T, Ruan J, Homer N, Marth G, Abecasis G, Durbin R, Genome Project Data Processing S. 2009. The Sequence Alignment/Map format and SAMtools. Bioinformatics 25:2078-9.

67. Quinlan AR, Hall IM. 2010. BEDTools: a flexible suite of utilities for comparing genomic features. Bioinformatics 26:841-2.

68. Edgar R, Domrachev M, Lash AE. 2002. Gene Expression Omnibus: NCBI gene expression and hybridization array data repository. Nucleic Acids Res 30:207-10.

Figure 1

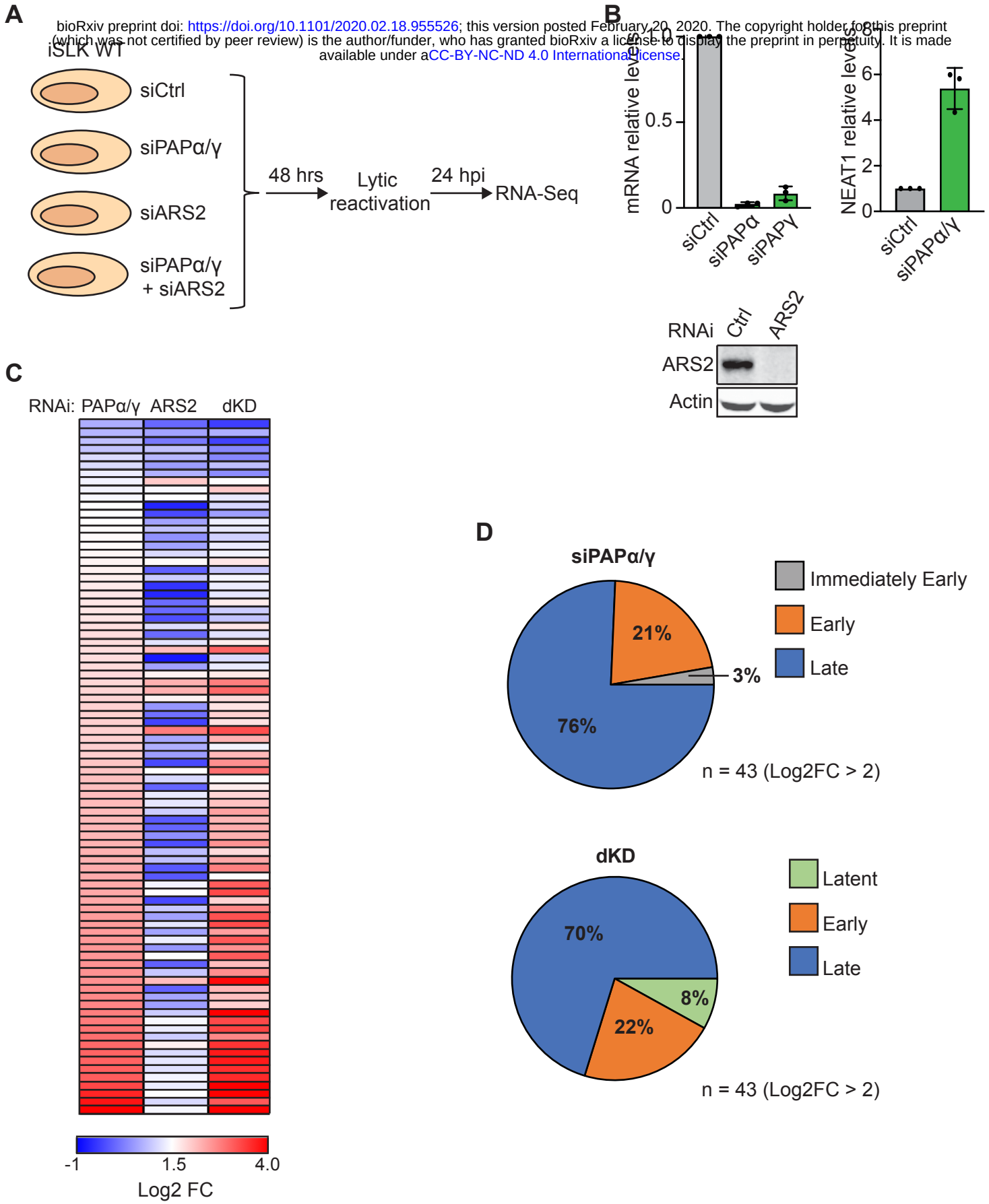

Figure 2

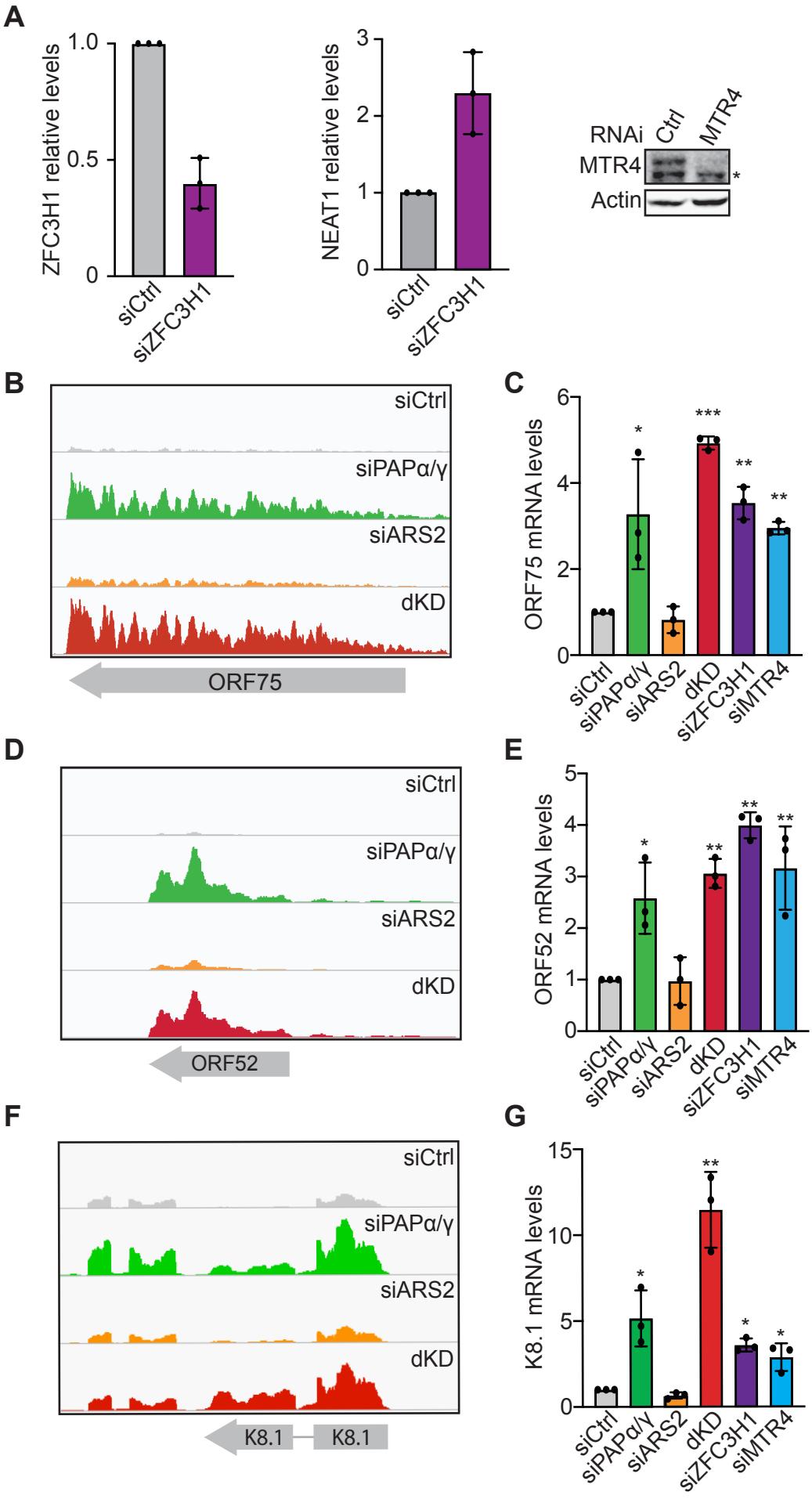

Figure 3

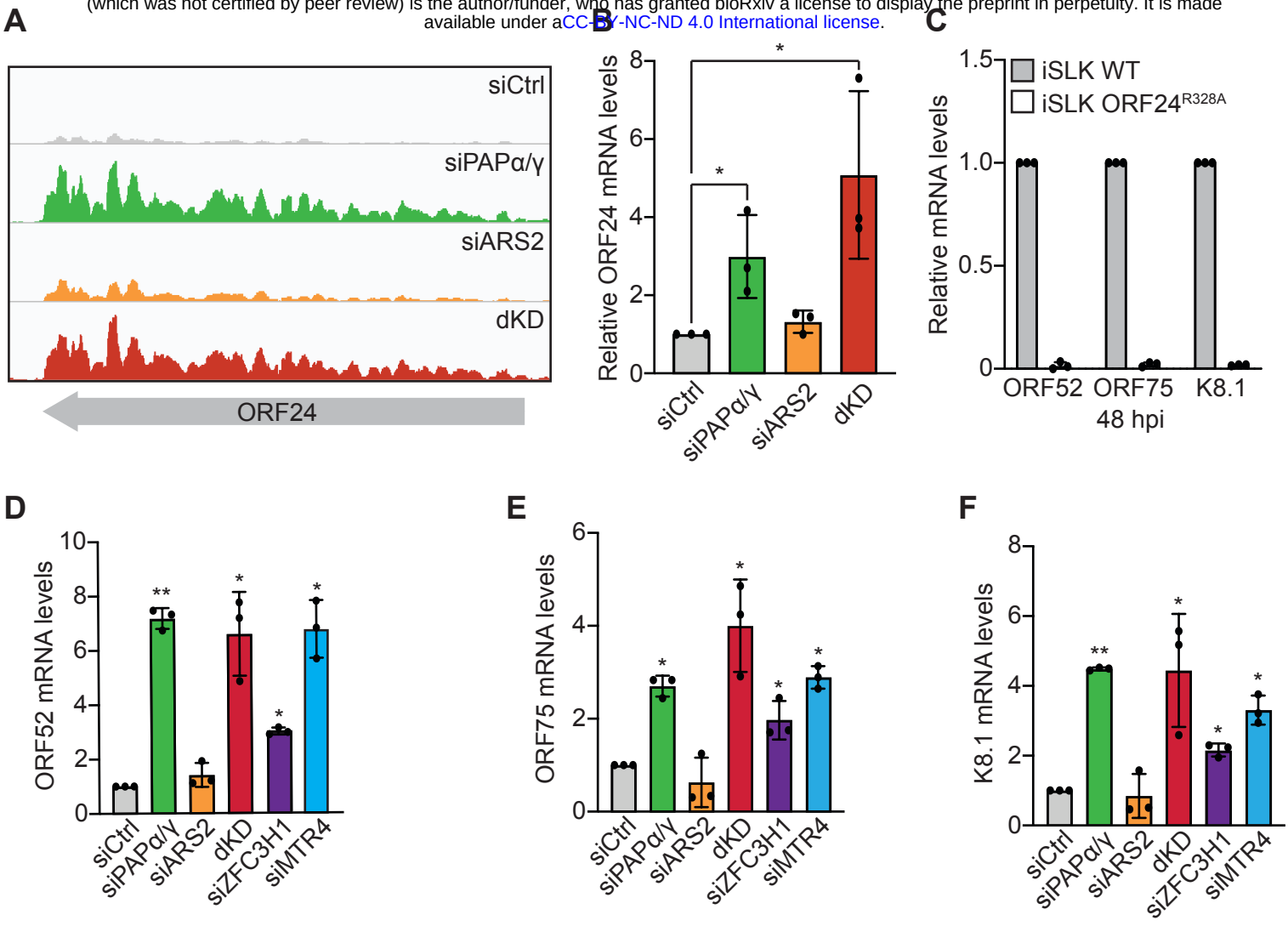

Figure 4

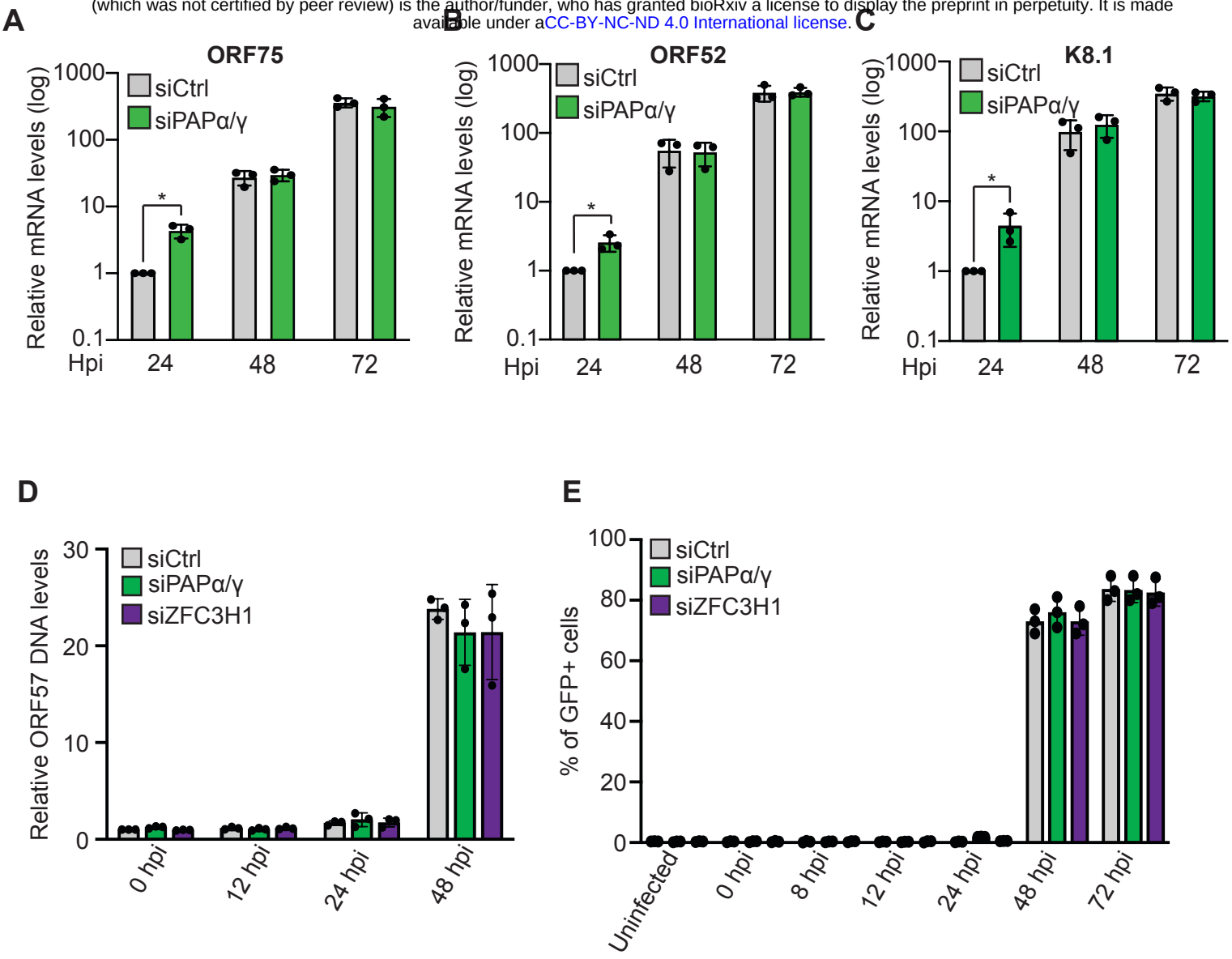

Figure 5

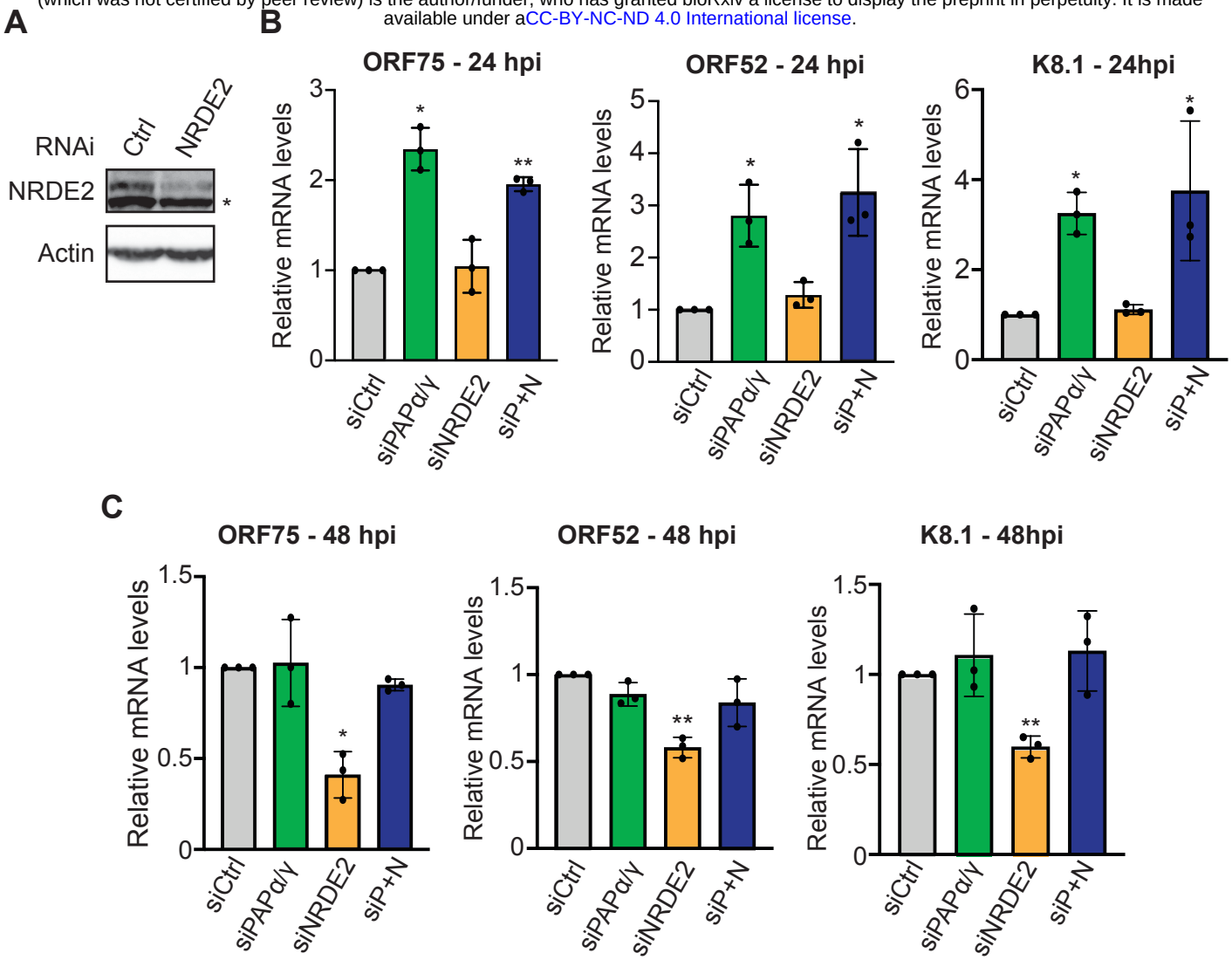

Figure 6